ELSEVIER

Nuclear Instruments and Methods in Physics Research A 410 (1998) 319–328

NUCLEAR INSTRUMENTS & METHODS IN PHYSICS RESEARCH Section A

Determination of HCNO concentrations by fast neutron scattering analysis

F.D. Brooks[a,*], A. Buffler[a], M.S. Allie[a], K. Bharuth-Ram[b], M.R. Nchodu[a], B.R.S. Simpson[c]

[a] *Physics Department, University of Cape Town, Rondebosch 7700, South Africa*
[b] *Physics Department, University of Durban-Westville, Durban 4000, South Africa*
[c] *National Accelerator Centre, P.O. Box 72, Faure 7131, South Africa*

Received 4 July 1997; received in revised form 3 November 1997

Abstract

A technique has been developed whereby a pulsed, monoenergetic fast neutron beam is used to determine concentrations of the elements H, C, N and O in small (0.2–1 kg) samples. Organic scintillators detect neutrons scattered by the sample and pulse height and time-of-flight data recorded by the detectors are analysed using the HEPRO program system (PTB, Braunschweig). Test measurements on compounds of the four elements show that atom fractions and masses may be determined to a few percent accuracy.

PACS: 29.30Hs; 28.20Cz

Keywords: HCNO analysis; Fast neutron scattering; NE230 scintillator; Contraband detection

1. Introduction

In recent years there has been considerable interest in possibilities for using fast neutron beams as probes for examining medium or large packages (0.5 m^3 or larger) non-intrusively [1–11]. Much of this interest relates to the need for more effective methods for detecting hidden contraband such as narcotics or explosives, for example in airline baggage or cargo containers. Three distinct factors make neutrons of energy 0.1–10 MeV promising candidates for this application. Firstly, neutron beams in this energy range can penetrate 1–2 m into a "typical" package of baggage or cargo without being too severely attenuated. Secondly, the interactions of neutrons with material are very sensitive to the neutron energy and the nuclides in the material, and this makes it possible to determine these nuclides (and hence the corresponding chemical elements) by monitoring the neutron interactions in various ways. Thirdly, the principal constituents of narcotic and explosive materials are the elements hydrogen, carbon, nitrogen and oxygen (HCNO), which differ strongly from one-another in their interactions with neutrons and can thus be characterised via these differences [5].

* Corresponding author. E-mail: fdb@uctvms.uct.ac.za.

0168-9002/98/$19.00
PII S0168-9002(98)00264-2

Two methods for fast neutron interrogation that have been thoroughly explored and are now being implemented are the fast neutron transmission spectroscopy method (FNTS) [6–10] and the pulsed fast neutron analysis method (PFNA) [1–4]. The FNTS method is based on measurements of the attenuation of a pulsed fast neutron beam passing through the interrogated material. The PFNA method uses a pulsed monoenergetic neutron beam and measures the energy spectrum and time of arrival of prompt gamma rays which are excited by inelastic neutron scattering in the interrogated material. Different elements are identified via their characteristic gamma spectra in this method and the time measurement is used to locate the position of the scatterer.

An alternative approach which has received comparatively little attention to date is to use a pulsed monoenergetic incident neutron beam and to detect, *directly*, the neutrons scattered out of the beam [11–13]. Four possible methods are suggested for identifying and measuring nuclides in this way, and they can be used individually or in combination. Firstly, if the energy of elastically backscattered ($> 150^{\circ}$) neutrons can be measured sufficiently accurately then the kinematics of this process provides a basis for determining the mass of the scattering nuclide. The operating principle is the same as that underlying the well-known technique of Rutherford backscattering analysis, in which monoenergetic charged particle beams are used to investigate surface regions of solids. Secondly, if inelastic neutron scattering is significant then this will add a low-energy component to the scattered neutron spectrum, which may characterise the scatterer. Thirdly, if the incident energy is suitably chosen and scattered neutrons are measured at two angles, one forward (e.g. 45°) and the other backward, then the ratio of the forward and backward scattering may be an indicator of the scattering nuclide. Fourthly, if one or more of the measurements listed above is made at two suitably chosen incident neutron energies, then characteristic variations in scattering cross sections with neutron energy may also facilitate identification of the scattering nuclides. Preliminary studies suggested that incident neutron energies 6.8 and 7.5 MeV might be used in this way to identify scattering from the elements C, N and O.

We report here on studies to investigate the feasibility of using the technique of fast neutron scattering analysis (FNSA), based on the ideas outlined above, to determine element concentrations in small samples (> 0.2 kg). These investigations form the first part of a more extensive study and were made with the limited objective of determining the extent to which the FNSA method is capable of determining concentrations of the elements H, C, N and O in samples of materials composed exclusively of these elements.

2. Experiments

The experimental arrangement used for scattering studies is shown schematically in Fig. 1. Pulsed 7.5 MeV neutrons were obtained by directing the pulsed 4.7 MeV deuteron beam DB through a 3 μm havar window into the 30 mm long target cell TG, filled with deuterium gas at 1.0 atm pressure. Measurements were also made at the alternate neutron energy 6.8 MeV by dropping the deuteron energy to 4.0 MeV. The pulsed deuterons (FWHM < 2 ns, repetition frequency 2 MHz, mean current 1 μA) were supplied by the CN Van de Graaff accelerator of the National Accelerator Centre (NAC), Faure, South Africa, which is equipped with a klystron bunching system.

Neutrons emitted along the line NB, at 0° relative to the deuteron beam DB, were used for the

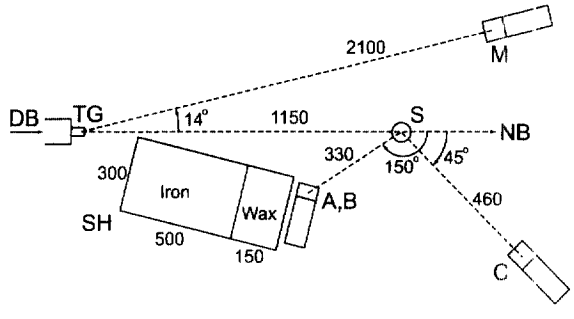

Fig. 1. Schematic diagram of the arrangement used for scattering measurements, showing the pulsed deuteron beam (DB), deuterium gas target (TG), shadow shield (SH), neutron beam (NB), scattering sample (S) and liquid scintillator detectors (A, B, C and M). Point-to-point distances are indicated in mm.

scattering studies. The incident neutron intensity was monitored by the NE213 scintillator M (50 mm $\phi \times 50$ mm). Most of the scattering samples S were powders or liquids held in thin, cylindrical aluminium cans (60 mm $\phi \times 110$ mm, mass 40 g) which were suspended with their axes perpendicular to the incident neutron direction NB. The neutron detectors A and B, positioned one above the other at scattering angle 150° relative to S, were liquid scintillators (40 mm $\phi \times 30$ mm) of NE213 and NE230 (deuterated), respectively. These two types of scintillator were compared as alternatives for the backscattered neutron detector. Deuterated scintillators are considerably more expensive than a natural organic scintillators such as NE213 but might nevertheless be the preferred if their performance should prove sufficiently superior for this application. Detector C was an NE213 scintillator (50 mm $\phi \times 50$ mm). The iron and wax shadow bar SH shielded detectors A, B and C from neutrons emitted directly from the neutron source TG and from collimators associated with the deuteron beam DB. Pulse shape discrimination was used on all four detectors (A, B, C and M) to select neutrons and reject gamma rays.

2.1. Calibration measurements

The response functions (pulse height spectra) of detectors A, B and C for monoenergetic neutrons were individually measured by moving the respective detectors temporarily into the beam NB at the sample position S in Fig. 1 and applying a neutron time-of-flight gate to select neutrons at beam energy. Fig. 2 shows the response functions obtained for detectors A and B for 6.8 and 7.5 MeV neutrons. The spectra show features expected [13] for the respective detectors, notably the approximately flat pulse height distributions from A and the peaked distributions from B. The maxima in the B spectra (Fig. 2b and d) arise from the enhanced probability for forward deuteron recoil in n-d elastic scattering, the dominant detection mechanism in this scintillator at these energies. The upper limits (edges) of the L-spectra, which correspond to forward recoil of protons in A, or deuterons in B, increase with neutron energy, as expected, and the slight enhancements visible just below the edges can be attributed [13] to the effects of multiple neutron scattering in the scintillators. The slopes of these edges provide a measure of the pulse height

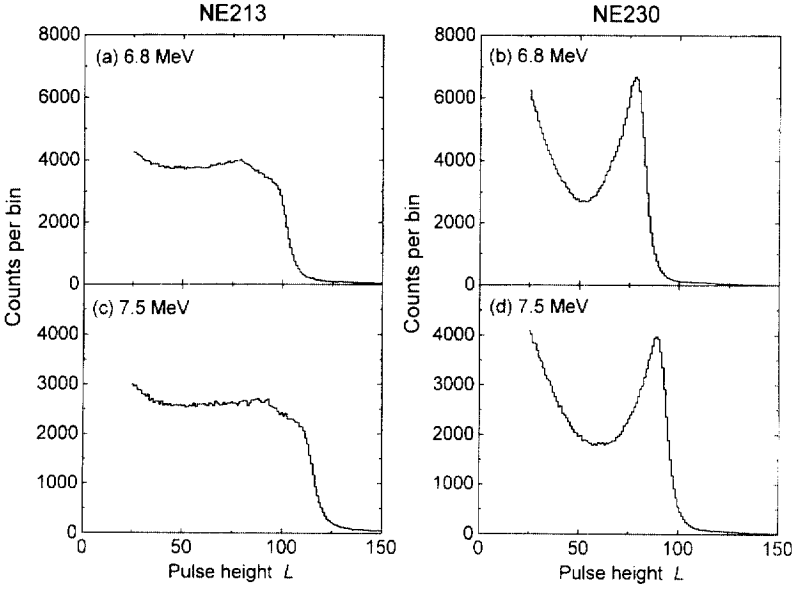

Fig. 2. Pulse height response functions measured for NE213 detector A and NE230 detector B, for neutrons of energy 6.8 and 7.5 MeV, as indicated.

resolution of the detectors. This is found to be about 5% (FWHM) for both detectors, in agreement with previous measurements [13]. Response functions were also measured for detector C at 6.8 and 7.5 MeV.

2.2. Scattering measurements

The arrangement shown in Fig. 1 was used to measure pulse height and time-of-flight distributions from detectors A, B and C for neutrons scattered from a variety of different scatterers S. Pulse height L and time-of-flight T data were captured simultaneously from the three detectors and written event-by-event to disk, for subsequent off-line analysis. The analysis of the scattering data obtained using detector A is not yet complete, therefore we concentrate, in this paper, on the backward and forward scattering measurements made using detectors B and C alone. Fig. 3 shows a perspective display of counts from detector B as a function of L and T. The data were obtained by scattering 7.5 MeV incident neutrons on a graphite sample (50 mm $\phi \times 100$ mm). The principal features (Fig. 3) are the ridges E and I. Ridge E is attributed to neutrons scattered elastically by carbon, which enter B with energy 5.5 MeV. Ridge I is attributed to neutrons which scatter inelastically, populating the 4.43 MeV level of ^{12}C, and arrive at B with energy 1.8 MeV. The pulse height spectrum for neutrons elastically scattered at 150° from graphite may be obtained by projecting the events within the time-of-flight window W_T (selecting ridge E) onto the pulse height axis L. It can be seen that this spectrum will be similar in form to those shown in Fig. 2b and d. For C, N or O scatterers the edge (upper limit) of the projected spectrum corresponds to the forward recoils caused by neutrons of energy equal to the incident energy multiplied by the kinematic factors 0.729, 0.763 or 0.789, respectively. We have previously shown [13] that CNO contributions can be resolved from the edge pulse height shifts in projected spectra of this type.

The scattering yield measured by detector C (at 45°) for 7.5 MeV neutrons incident on graphite shows features similar to those for detector B when presented as in Fig. 3, and also displays ridges corresponding to elastically scattered neutrons

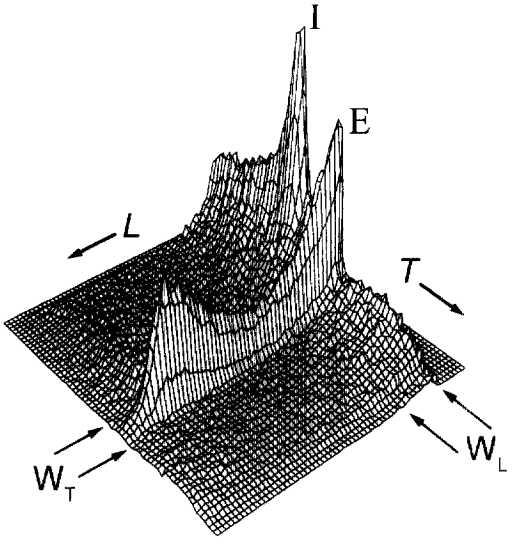

Fig. 3. Counts (vertical) as a function of pulse height L and time-of-flight T, measured by detector B for 7.5 MeV neutrons incident on a graphite sample, showing ridges due to elastically scattered neutrons (E) and inelastically scattered neutrons (I) associated with excitation of the 4.43 MeV level of ^{12}C. The time window W_T and the pulse height window W_L referred to in the text are shown.

(7.1 MeV) and inelastically scattered neutrons (2.8 MeV), respectively. At this angle the energy variations between elastically scattered neutrons from C, N and O are very small ($< 2\%$). Therefore, unlike the case at 150°, measurements of pulse height only (from a liquid scintillator) are not sufficient to separate these elements from one-another. The forward scattering measurements are nevertheless particularly useful in two important ways. Firstly, the ratio of forward-to-backward scattering may be useful, as previously noted. Secondly and most importantly, scattering (other than multiple scattering) from hydrogen is kinematically confined to forward angles and is characterised (and therefore also distinguished) by a significant energy loss. For example, at laboratory angle 45° the neutron energy is halved after elastic scattering on H. Thus in a plot such as Fig. 3, but obtained using detector C and a sample containing hydrogen as well as carbon, one observes an additional ridge between ridges E and I, due to elastic scattering on H. To derive a convenient signature from measurements by detector C we define a pulse height window

W_L at low pulse heights (see Fig. 3) and project events within this window onto the T-axis. The elastic and inelastic ridges E and I contribute peaks to this projected T-spectrum and any hydrogen in the scatterer contributes an additional peak which lies between these two peaks.

3. Neutron scattering signatures

The neutron scattering information which is most useful for identifying the scattering nuclide is thus concentrated in two areas: firstly in the edge region of the projected pulse height spectrum observed for elastically backscattered neutrons selected by the time window W_T in Fig. 3; and secondly in the projected time spectrum selected by a low pulse height window applied to the neutron detector C, which detects forward scattered neutrons. We combine these components as shown in Fig. 4 to define a compact, single "*scattering signature*" for each sample studied. Fig. 4 shows (as histograms) signatures obtained from scattering measurements on samples of: (a) graphite; (b) liquid nitrogen; and (c) water. A spherical glass dewar flask of volume 1.00 l held the liquid nitrogen in measurement (b). Each signature in Fig. 4 consists of two sections: channels 1–200 on the left, derived from the measurements at 6.8 MeV; and channels 201–400 on the right, derived from the measurements at 7.5 MeV. In each section the first 140 channels incorporate a component extracted from the projected L-spectrum measured by detector B (150°) and the last 60 channels incorporate a component extracted from the projected T-spectrum measured by detector C (45°). The extracted L-component extends from well-below to well-above the region in which pulse height edges are observed for C, N and O scattering. The extracted T-component includes the peaks corresponding to ridges I and E in Fig. 3. Each signature is thus a 400-channel distribution, $S(n)$ for $n = 1$–400, which contains energy and angular distribution information about the scattering of 6.8 and 7.5 MeV neutrons on the nuclides of the associated sample. The scales for $S(n)$ in Fig. 4 have been normalized so as to correspond to the counts that would be registered for a standard number of incident neutrons (indicated by a standard count

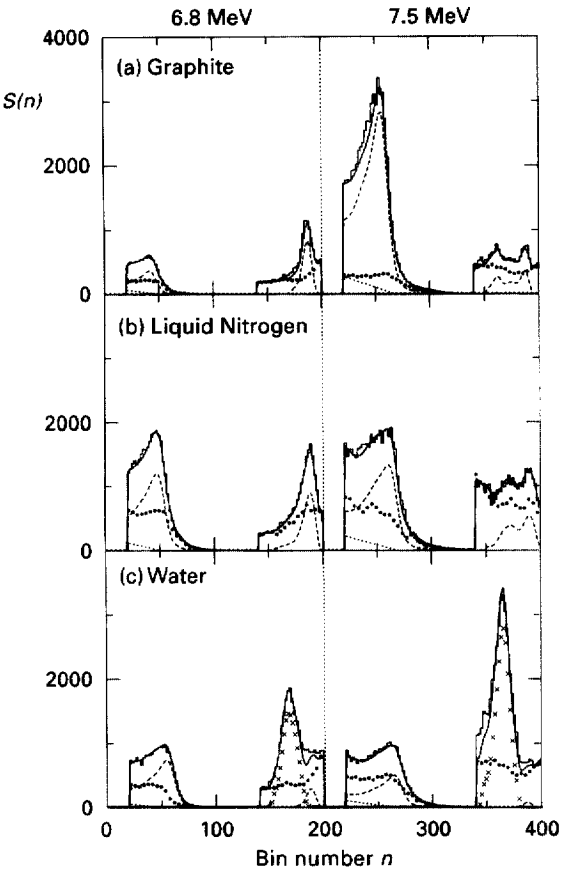

Fig. 4. Measured scattering signatures $S(n)$ (histograms) for (a) graphite, (b) liquid nitrogen and (c) water samples, and fits obtained using the code HEPRO (solid curves). Dashed curves show the C, N and O signature components fitted by HEPRO. Crosses in (c) show the H-signature component fitted by HEPRO. Points show measured backgrounds and dotted linear components show multiple scattering contributions fitted by HEPRO. All measurements are normalized to the standard neutron monitor count and to $100N_A$ target nuclei in the scattering sample, where applicable.

from the monitor M) and to a standard number of $100N_A$ target nuclei (C, N or O) in the scatterer, where N_A is Avogadro's number. The background signatures plotted as points in Fig. 4 are also normalized to the standard number of monitor counts and were obtained from measurements made using either an empty aluminium container (Fig. 4a and c) or the empty dewar (Fig. 4b) at the sample position S (Fig. 1).

The signatures $S(n)$ in Fig. 4 illustrate some important features which underlie the proposed technique of fast neutron scattering analysis (FNSA) for determining concentrations of the elements H, C, N and O in a scattering sample. Firstly, the small but significant increase of the edge pulse height on progressing from C to N and then to O can be seen, showing that backscattering measurements can resolve these elements from one-another. Secondly, after subtracting background, the change in intensity of both back- and forward-scattered neutrons with increase in incident neutron energy is seen to differ for the three elements. The projected T-components also vary with incident neutron energy in a way which is distinctive for different elements and the expected hydrogen peaks appear strongly in the signature measured for water (Fig. 4c).

3.1. Signatures for the elements H, C, N and O

The scattering signatures measured for the three samples listed in Fig. 4, and the associated background measurements (points), provide data from which scattering signatures for the component elements, H, C, N and O, of these samples can be derived. For the single-element samples, graphite and nitrogen, the C or N signature may be obtained, in principle, simply by subtracting the normalized background. A different procedure was followed however, in order to obtain better statistical accuracy and to make some allowance for the effects of multiple neutron scattering on the measurements.

3.1.1. The C-signature

Each signature in Fig. 4 was considered in two parts, corresponding to the 6.8 and 7.5 MeV sections respectively. In fitting the graphite measurement (Fig. 4a) we assume that, in the absence of multiple neutron scattering, the L-component of the *carbon* signature (each section) should have the same form as the response function (Fig. 2b or d) of detector B and can therefore be simulated by rebinning (re-distributing) this response function so as to match its edge pulse height to that observed in the scattering measurement (Fig. 4a). Noting further that multiple neutron scattering may be expected to enhance the low energy region of the scattered neutron spectrum at the expense of the high energy region, we assume, arbitrarily, that multiple scattering may be represented to first approximation by an additional component which decreases linearly with increasing L. The L-component in each graphite signature (Fig. 4a) was therefore fitted by a sum of the following three components: the detector response function, rebinned as described above to represent the form of the carbon signature; a smoothed background function based on the background data shown in Fig. 4; and a linear component to approximate the effect of multiple scattering. The T-component in each signature was fitted simultaneously with its associated L-component, after smoothing the experimentally measured backgrounds for the T-components in the same way as used for the L-components. Gaussian functions were used to fit the elastic and inelastic scattering peaks in the T-components. Fitting was carried out using the HEPRO program system [14–16]. The results obtained for the 6.8 and 7.5 MeV sections were then combined, giving the fit shown by the solid line in Fig. 4a and the carbon signature shown by the dashed line in the same figure.

3.1.2. The N-signature

The signature for nitrogen was derived from the data shown in Fig. 4b by following the same procedure as used for carbon, but with some important modifications demanded by the presence of inelastic neutron scattering to the 2.3 MeV level of ^{14}N. The contributions of these inelastic neutrons to the T-components in Fig. 4b were dealt with in the same way as for the lower energy inelastic neutrons in the carbon signature. Due to their higher energy however, the neutrons scattered inelastically from nitrogen encroach more strongly than those from carbon on the time window W_T (Fig. 3), thereby contributing small but significant proportions of low-energy neutrons to the L-components of the nitrogen signature (Fig. 4b). To allow for this effect, the data of Fig. 4b were fitted using L-components which included both elastic and inelastic contributions. The inelastic neutrons introduce a second edge at lower pulse height, due to their lower energy. The proportion of inelastic component required in the nitrogen

signature was determined in the fitting and was found to be 5% at 6.8 MeV and 8% at 7.5 MeV. The dashed curve in Fig. 4b shows the signature derived for nitrogen from the fitting.

3.1.3. The H and O signatures

The signatures for hydrogen and oxygen were obtained from the data taken using the water sample, knowing that hydrogen makes strong and distinctive contributions to the T-components of the water signature (Fig. 4c) but no contribution to the L-components. The water signature was first fitted using HEPRO, following the same procedure as used for the carbon signature. The peaks due to hydrogen in the resulting fits (for 6.8 and 7.5 MeV, respectively) were then identified and extracted to form the H signature. The residual fit, after removal of these peaks, gave the signature for O. The components indicated by crosses and dashed lines in Fig. 4c show the signatures derived for H and O, respectively.

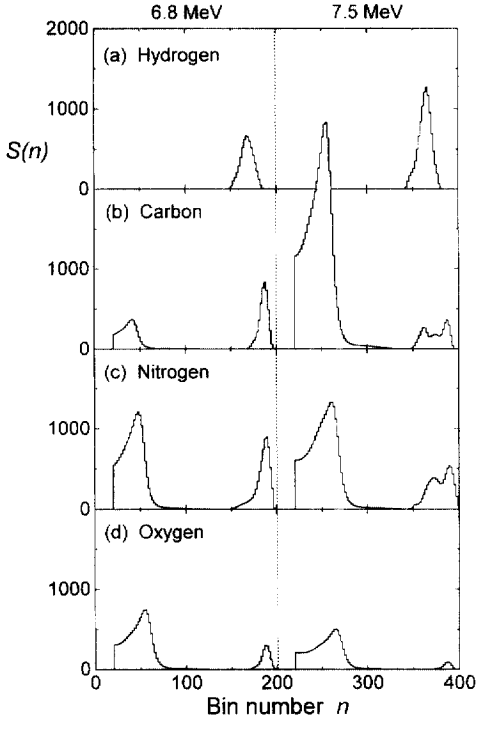

Fig. 5. Scattering signatures $S(n)$ for H, C, N and O (normalized to the standard neutron monitor count and to $100N_A$ target nuclei in the scatterer).

The signatures obtained for the four elements are summarised in Fig. 5. The signature for H is reduced by a factor of 2 relative to that shown in Fig. 4c, due to the 2 : 1 ratio of H : O nuclei in water. These signatures, together with the smoothed background signature functions and the assumed linear multiple scattering components already referred to, formed the response matrix required for use in conjunction with the code HEPRO as discussed below. The FNSA method relies on the assumption that the relative intensities of the H, C, N and O signatures required to make such a fit will be proportional to the atom fractions of the corresponding elements in the scatterer. To test and demonstrate the FNSA method we present measurements and analyses made on some additional compounds of the elements H, C, N and O.

4. Tests of FNSA on HCNO compounds

Scattering signatures were measured as outlined above for anhydrous samples of the four compounds, methanol, ammonium nitrate, ammonium acetate and acetamide. Each signature was analysed, using HEPRO, into components corresponding to the elements H, C, N and O, background components and multiple scattering components. The signatures measured for the four compounds, normalized to the standard number of monitored incident neutrons, are shown as histograms in Fig. 6. The fits to the signatures are shown by the solid curves in Fig. 6. Background and multiple scattering components are indicated by dashed and dotted curves respectively, and the H, C, N and O components are shown by crosses, solid circles, triangles and open circles, respectively.

For each compound, the scattering signature $S(n)$, is given by

$$S(n) = \sum_{i=1}^{8} f_i S_i(n) \qquad (1)$$

in which the functions $S_i(n)$ correspond to the following: $i = 1$–4, the scattering signatures for elements H, C, N and O, respectively; $i = 5$ and 6, the smoothed background functions at 6.8 and

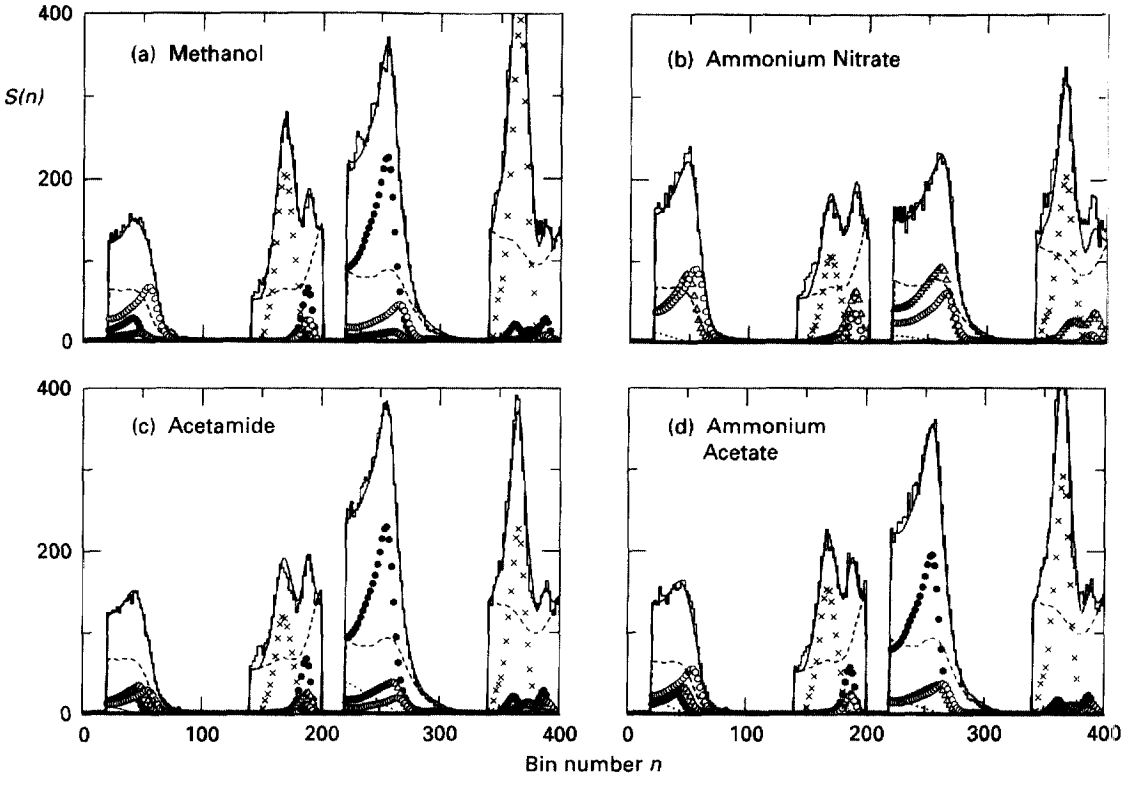

Fig. 6. Measured scattering signatures $S(n)$ (histograms) and HEPRO fits (solid curves) for samples of (a) methanol, (b) ammonium nitrate, (c) acetamide and (d) ammonium acetate. Dashed and dotted curves show the smoothed backgrounds and linear multiple scattering components determined in the HEPRO fitting. The H, C, N and O components determined in the fitting are shown by crosses, solid circles, triangles and open circles, respectively.

7.5 MeV, respectively; and $i = 7$ and 8, the linear functions used to describe multiple scattering contributions at 6.8 and 7.5 MeV respectively. The coefficients f_i are determined, using HEPRO, when the scattering signature $S(n)$ is fitted.

Since the element signatures $S_i(n)$ for $i = 1$–4 (Fig. 5) are normalized so as to correspond to a scatterer containing $100N_A$ nuclei of the element i, the fitting factor f_i determined in the analysis indicates the presence of $100 f_i N_A$ nuclei of this element in the scatterer. The total number of HCNO nuclei in the scatterer is thus given by

$$N_{tot} = 100 N_A \sum_{i=1}^{4} f_i \tag{2}$$

and the atom fraction a_i for element i, defined as the fraction of these HCNO nuclei that are nuclei of this element, is given by

$$a_i = f_i \Big/ \sum_{i=1}^{4} f_i \tag{3}$$

The mass M of the scattering sample, in kg, is given by

$$M = 0.1 \sum_{i=1}^{4} f_i A_i \tag{4}$$

where A_i is the mass number of nuclide i.

Atom fractions and sample masses determined from Eqs. (3) and (4), using the f_i data determined from the HEPRO fits, are listed in Table 1, together with known values of a_i and M determined from chemical formulae and by weighing, respectively. The measured and calculated values of a_i may also be compared with one-another in the plot presented in Fig. 7. The agreement between

Table 1
Atom fractions and masses for samples of four HCNO compounds

Sample [Formula]	Atom fractions a_i				M
	H	C	N	O	(kg)
Methanol	0.633 (24)	0.163 (10)	0.018 (8)	0.186 (12)	0.285 (13)[a]
$[H_4\ C\ O]$	0.667	0.167	0	0.167	0.288[b]
Ammonium nitrate	0.455 (23)	0.003 (3)	0.198 (8)	0.345 (25)	0.311 (15)[a]
$[H_4\ N_2\ O_3]$	0.444	0	0.222	0.333	0.298[b]
Acetamide	0.544 (12)	0.246 (24)	0.088 (15)	0.122 (18)	0.220 (15)[a]
$[H_5\ C_2\ N\ O]$	0.555	0.222	0.111	0.111	0.212[b]
Ammonium acetate	0.574 (45)	0.172 (10)	0.067 (17)	0.187 (10)	0.264 (13)[a]
$[H_7\ C_2\ N\ O_2]$	0.583	0.167	0.083	0.167	0.272[b]

[a]Calculated from f_i values determined using HEPRO.
[b]Calculated from chemical formula (a_i) or determined by weighing (M).

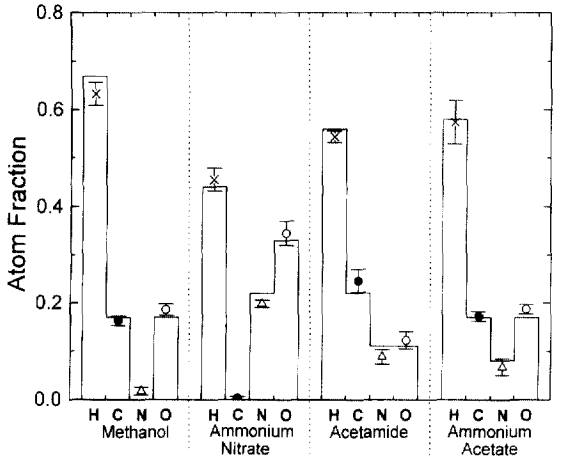

Fig. 7. Measured values (points) and calculated values (histograms) of the atom fractions a_i for the four compounds listed in Fig. 6 and Table 1.

the measured and known values is excellent for both a_i and M.

5. Discussion

The results presented in Table 1 and Fig. 7 demonstrate that the combination of scattering signature measurements of the type described here with the unfolding analysis available through use of the code HEPRO is very effective for identifying and measuring concentrations of the elements H, C, N and O. This indicates that the FNSA method, or possibly a variation of this method based on a differently defined signature, could be developed into a useful non-intrusive neutron interrogation system for small packages. Further work is now in progress to explore this possibility. The work includes investigations of, for example, effects arising from the attenuation of neutrons in the interrogated material before and after scattering, the effects of multiple neutron scattering and techniques that could be used to locate different scattering centres in an extended sample volume. Measurements have already been made using scattering samples which include additional elements outside the range $6 \leq Z \leq 8$. Analyses already completed on the data obtained from these measurements indicate that the FNSA method for HCNO is not impaired by the presence of other elements and that it promises to be useful over a wide range of A.

The time required to complete the interrogation of a typical package, for example of volume 0.5 m^3, will clearly be a critical consideration in determining whether a FNSA system is suitable for practical implementation. The data required to answer this question should also be provided from the investigations now in progress, which include studies of the methods most suitable for improving the

solid angle coverage and efficiency of the detection system. The preliminary analyses already completed on data taken using the NE213 liquid scintillator, detector A (Fig. 1), indicate that this type of detector is also likely to be suitable for use in the FNSA system, though not quite as effective as the NE230 detector B.

Acknowledgements

We thank the following for the support they have rendered to us in carrying out this work: Dr. M. Matzke of PTB, Braunschweig, Germany, for providing the HEPRO code and for guiding us in its application; D. Momsen, D. Boulton and G. Fowle for their technical assistance; the staff of the Van de Graaff group at NAC, Faure, for their assistance in running the experiments; and the International Atomic Energy Agency, Vienna, and the South African Foundation for Research Development, for financial support.

References

[1] T. Gozani, Nucl. Instr. and Meth. A 353 (1994) 635.
[2] Z.P. Sawa, Nucl. Instr. and Meth. B 79 (1993) 593.
[3] T. Gozani, Proc. SPIE 2867 (1997) 174.
[4] D.R. Brown, T. Gozani, R. Loveman, J. Bendahan, P. Ryge, J. Stevenson, F. Liu, M. Sivakumar, Nucl. Instr. and Meth. A 353 (1994) 684.
[5] G. Vourvopoulos, Nucl. Instr. and Meth. B 89 (1994) 388.
[6] J.C. Overley, Nucl. Instr. and Meth. B 24/25 (1987) 1058.
[7] J.C. Overley, Int. J. Appl. Radiat. Isot. 36 (1985) 185.
[8] J.C. Overley, M.S. Chmelik, R.J. Rasmussen, G.E. Sieger, R.M.S. Schofield, H.W. Lefevre, Proc. SPIE 2867 (1997) 219.
[9] H.W. Lefevre, R.J. Rasmussen, M.S. Chmelik, R.M.S. Schofield, G.E. Sieger, J.C. Overley, Proc. SPIE 2867 (1997) 239.
[10] T.J. Yule, B.J. Micklich, C.L. Fink, L. Sagalovsky, Proc. SPIE 2867 (1997) 206.
[11] H.J. Gomberg, G.B. Kushner, in: S.M. Khan (Ed.), Proc. 1st Int. Symp. on Explosive Detection Technology, Atlantic City Airport, November 1991, Federal Aviation Administration publication DOT/FAA/CT-92/11, pp. 123.
[12] F.D. Brooks, C.G.L. Henderson, M.S. Allie, A. Buffler, M.J. Oliver, M.R. Nchodu, D.T.L. Jones, B.R.S. Simpson, F.D. Smit, J.E. Symons, Proc. SPIE 2339 (1995) 431.
[13] A. Buffler, K. Bharuth-Ram, F.D. Brooks, M.S. Allie, M. Herbert, M.R. Nchodu, B.R.S. Simpson, Proc. SPIE 2867 (1997) 192.
[14] K. Wiese, M. Matzke, Nucl. Instr. and Meth. A 280 (1989) 103.
[15] M. Matzke, Unfolding of pulse height spectra: the HEPRO program system, PTB Braunschweig Report PTB-N-19, 1994.
[16] M. Matzke, Proc. SPIE 2867 (1997) 598.